Int. J. Electrochem. Sci., 13 **(2018)** 5204 – 5218, doi: 10.20964/2018.06.09

International Journal of
ELECTROCHEMICAL
SCIENCE
www.electrochemsci.org

Nitrogen-rich Porous Carbon Derived from Biomass as High Performance Electrode Materials for Supercapacitors

JianQiang Zhang[*], *SenYang Song, JieChen Xue, Ping Li, ZhiShang Gao, YanBo Li, Zheng Zhang, HuiXia Feng and HeMing Luo*

College of Petrochemical Technology, Lanzhou University of Technology, Lanzhou 730050, PR China.
[*]E-mail: zhangjq@lut.cn, luohm666@163.com

Received: 31 December 2017 / *Accepted:* 24 February 2018 / *Published:* 10 May 2018

In situ nitrogen doped porous carbon materials (NC) has been architectured vis hydrothermal - carbonization coupling method by the nitrogen-rich biomass, black garlic (BG). The resulting NC performs a high specific surface area, above 2000 m^2 g^{-1} with abundant mesoporous and microporous hierarchical structure, as well as a high graphitization degree demonstrated by XRD and Raman. Further electrochemical measurements revealed that the corresponding electrode prepared by these NC can lead to a significantly high specific capacitance of 331 F g^{-1} in a 6 M KOH aqueous electrolyte, which is higher than other porous carbon materials obtained by most biomass. Furthermore, the corresponding electrode shows a high degree of cycling stability. This contribution shows that the NC derived from nitrogen-rich biomass are more environmental-friendly and less energy consuming than that of nitrogen doped carbon materials obtained from other conventional methods. Also, the effect of hydrothermal treatment has been discussed relative to the conventional one-step carbonization.

Keywords: In situ doped, nitrogen doped, porous carbons, black garlic, supercapacitors

1. INTRODUCTION

Supercapacitors known as a promising electrochemical energy storage devices with high power density, excellent cycling stability and high specific capacitance characteristics, which have specific applications such as electric vehicles, backup energy, consumer electronics and even to replace batteries[1-5]. According to the different energy storage mechanism, supercapacitors can be divided into two major categories: electrochemical double-layer capacitor (EDLC) and pseudocapacitor. EDLC stores electrical energy by separation of charge in a Helmholtz double layer, pseudocapacitor stores electrical energy by faradaic redox reactions with charge-transfer. Compared with pseudocapacitor, EDLC mainly use porous carbon electrode with large specific surface, such as carbon nanotubes,

graphene and activated carbon (AC), which charges or ions are stored in the double-layer on the surface.. EDLC consist of two electrodes separated by an ion-permeable membrane, and an electrolyte ionically connecting both electrodes[6-8]. The performance of supercapacitor strongly depends on the composition, specific surface area, surface state, structure and conductivity of its electrode materials[9,10].

Porous carbon materials have a variety of preparation methods, such as high temperature pyrolysis activation method and template method. High temperature pyrolysis activation method proved to be a very economical and practical preparation method. Wang[11] use Onion husks as carbon source, K_2CO_3 as activator, prepared by high temperature pyrolysis carbonization method to obtain porous carbon material and shows an excellent electrochemical performance with large specific capacitance (about 188 F g^{-1} at 1 A g^{-1}). However, the capacitive properties of the porous carbon material obtained by the high-temperature pyrolysis activation method are not satisfactory. The comparison of the electrochemical performances between our results and other N-enriched carbon materials are listed in Table.S1.

In order to optimize the electrochemical properties of carbon materials, the introduction of heteroatoms in biomass carbon materials makes the pseudostructure effect of materials an effective way to increase the specific capacitance of the materials[12-14]. By doping N atoms in the carbon material can greatly change the surface structure of the material, adjust its pore structure, enhance its hydrophilicity, improve the material electron transport rate. The nitrogen-doped porous carbon has a better development prospect than the pure porous carbon with superior electrochemical properties[9,15]. After doping N atoms in the carbon material, the doping of N atoms produces a local tension in the hexagonal carbon network, resulting in structural deformation, and due to the additional solitary electrons of the N atom can bring the sp^2 hybrid carbon skeleton to delocalize π the system negatively charges, thereby enhancing the electron transport properties and chemical reactivity; at the same time to reduce the price of carbon material to enhance the chemical stability of carbon materials[16-18].

The chemical environment of N atoms in carbon materials is the key to controlling their properties. Typically, N in the carbon material is divided into two families: chemical nitrogen and structural nitrogen. Chemical nitrogen is present as a surface functional group, such as an amine, nitroso, and the like; and the structural nitrogen is directly attached to the carbon skeleton in the carbon material, such as pyridine type N, graphite type N[19-21]. Usually with ammonia, urea and nitric acid and other different nitrogen source heat treatment of various carbon materials, N atoms can be introduced into the carbon materials[22]. Shao[23] synthesize the pure porous carbon material by template method[24], then the nitrogen doped heat treatment was carried out with ammonia gas at high temperature, and the obtained nitrogen doped porous carbon material has a high specific surface area (1100 m^2 g^{-1}). However, these type of conventional nitrogen doped methods are energy-consuming and difficult to handle in the synthesis of carbon material by using N-containing precursors such as NH_3, acetonitrile, urea, etc. Therefore, to obtain a carbon material having a high content of structure N, it is usually a direct pyrolysis of a nitrogen-rich precursor (in situ doping method)[25]. The most commonly used nitrogen-rich precursors include such as melamine, benzylamine, N-containing heterocyclic compounds. Our previous work [26] use low-biotechnology fulvic acid potassium salts as

a precursor to synthesize nitrogen doped porous carbon materials, the obtained carbons had a high surface area (1623 m^2 g^{-1}) and good electrochemical properties (a capacitance of 235 F g^{-1} in a 6 M KOH aqueous solution). But the organic salt has a certain degree of chemical corrosion and toxicity. So it is important to select a green, non-toxic nitrogen-rich precursor.

Based on the ability to better enhance the traditional high temperature pyrolysis carbonization and nitrogen doping efficiency, We use nitrogen-rich biomass as carbon source, black garlic. As a kind of biomass, the garlic not only has a wealth of nutritional value and medicinal value, but cultivation area and high yield. Moreover, natural garlic will turn black after fermenting in which Maillard reaction happens[27]. The fermentation process is not the result of microbial fermentation, but refers to the physical and chemical reactions that occur after the destruction of the self-organization under the condition of high temperature and high humidity. In fermented garlic, protein content and carbohydrate content are much higher than that in natural garlic. In this contribution, a high specific surface area of nitrogen doped porous carbon (1714 m^2 g^{-1} under 800 °C) was prepared by hydrothermal-carbonization coupling method, which had a high specific capacitance (331 F g^{-1} at the current density of 1 A g^{-1}) and good cycle stability (the capacitance retention of 87.01 % over 5000 cycles). All these efforts show that nitrogen-rich biomass can be used as an in situ nitrogen doped carbon source, providing an economical and sustainable development for superelectric research. And related research is under way.

2. EXPERIMANTAL

2.1 Materials

Black garlic were purchased from food franchise stores. Acetylene carbon black was purchased from Shanxi Carbon Trading Co. Ltd. And all other chemicals including potassium hydroxide were analytical grade and were purchased from Tianjin BASF Chemical Co.Ltd.. All materials and chemical reagents were used as purchased without any further purification.

2.2 Synthesis of NC derived from black garlic

Black garlics were firstly washed and cut to cubes, followed by hydrothermal process at 180 °C for 10h. After that，pre-carbonized at 600 °C for 1.5 h under an argon atmosphere then mixed with 2 M KOH pyrolyzed at temperatures increasing up to 700, 800, and 900 °C for 2 h under an argon atmosphere with a heating rate of 5 °C /min. The resulting dark solid was ground to powder, washed with 1 M HCl solution, and then thoroughly washed with distilled water. The residue was collected and dried at 80 °C in a vacuum. The nitrogen doped carbon material through hydrothermal treatment followed by carbonization was denoted as BGNCT, in which BG represents black garlic, T represents carbonization temperature. As a comparison, the non-hydrothermal treatment BGNC was noted as NHBGNC to clarify the effect of hydrothermal process.

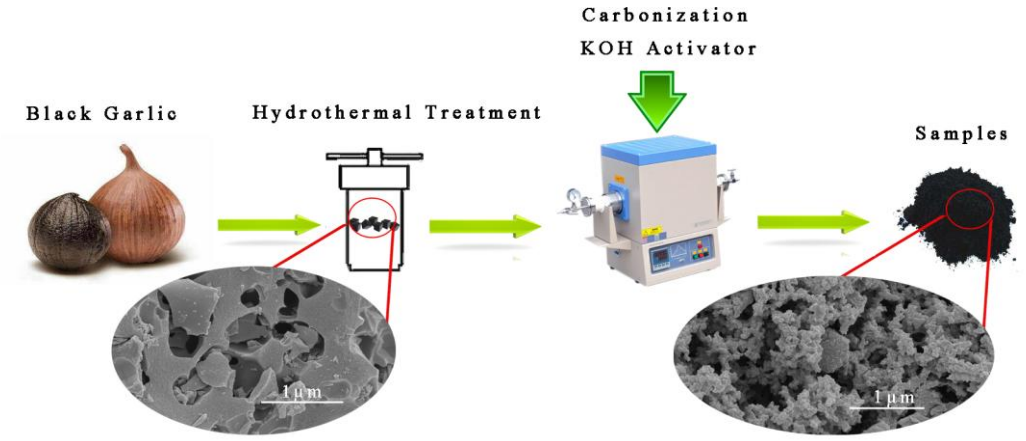

Figure 1. Scheme for the fabrication of the BGNC.

2.3 Characterization of the NC

The morphology and structure of the materials were characterized by field emission scanning electron microscopy (SEM; JSM-5600LV, JEOL) and high resolution electron microscopy (TEM; JEM-1200EX, JEOL). The Raman spectra of the materials were recorded by Horiva (JY-HR800 microRaman) spectrometer. The surface elemental composition analysis was detected by the X-ray photoelectron spectroscopy (VG scientific ESCA-3000 spectrometer). The crystalline structures and graphitization degree of the samples were characterized by powder X-ray diffraction (XRD; D/Max-2400, Rigaku). The surface area and pore size distribution were measured using N_2 adsorption (Micromeritics, ASAP 2020 analyzer).

2.4 Electrochemical measurements

All electrochemical characterizations were carried out on a CHI660c electrochemical workstation (Shanghai Chenhua Instruments Co.) at room temperature. To prepare the working electrode, a viscous slurry containing 80 wt% nitrogen-doped porous carbons material, 10 wt% carbon black, and 10 wt% polytetrafluoroethylene was mixed onto a nickel foam current collector. The as-formed electrodes (with a thickness of approximately 100 mm and an area of 1.0 cm^2) were then dried at 80 °C in a vacuum oven. After that, the working electrode was pressed at15 MPa for 1.5 min. The prepared NC loaded on the electrode is 4.0 mg for each electrode. In a three-electrode cell, the above loaded nickelfoam, a Pt wire and a Hg/HgO were used as the working, counter and reference electrodes. Cyclic voltammetry(CV) curves were obtained in the potential range of −1.0~0 V. By varying the scan rate from 10 to 100 mV s^{-1}. Electrochemical impedance spectroscopy (EIS) was measured in a frequency range of 10 kHz to 10 mHz at open circuit voltage with an alternate current amplitude of 5 mV. Charge–discharge measurements were done galvanostatically at 0.3~80 A g^{-1} over a voltage range of −1.0~0 V. For quantitative considerations, the specific capacitance was calculated from the galvanostatic charge–discharge values by using the following equation[28,29]:

$$C = \frac{I\Delta t}{m\Delta V} \qquad (1)$$

Where I (A) is the discharge current, ΔV (V) refers the potential change within the discharge time Δt (s), and m (g) represents the weight of active materials in the working electrode.

3. RESULTS AND DISCUSSION

3.1 Structural and morphological characterization

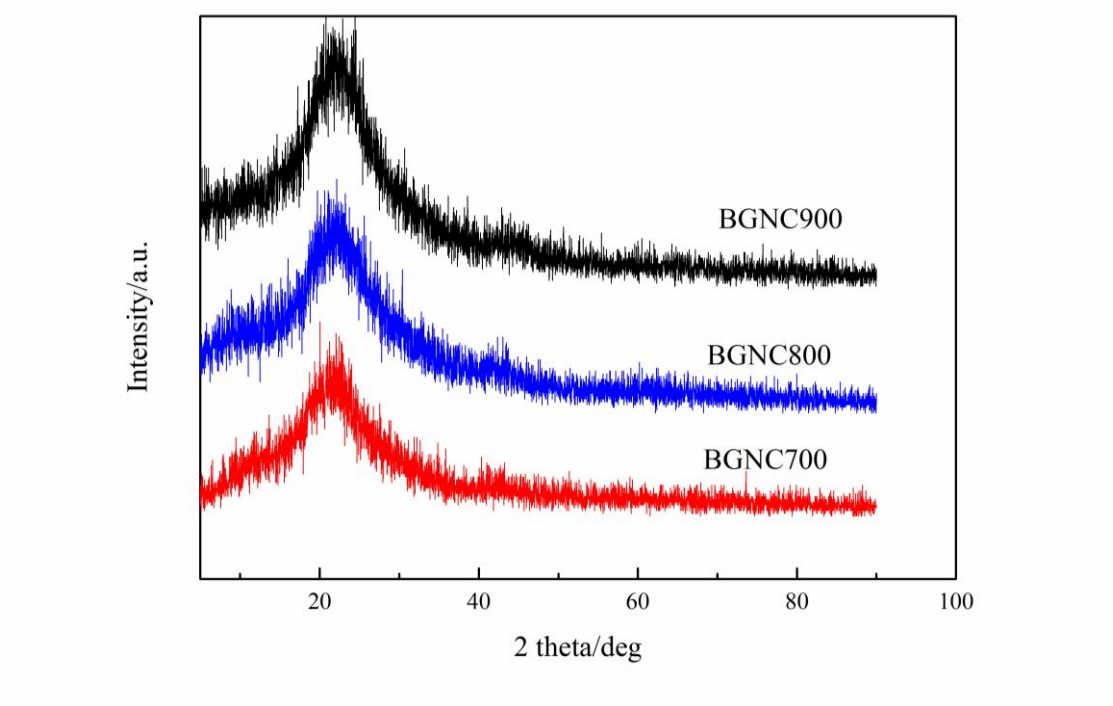

Figure 2. a Powder XRD patterns of BGNC samples.

The BGNC800 sample, which was obtained by black garlic, has the best electrochemical performance in the BGNC700/BGNC800/BGNC900 system. The XRD patterns of BGNC700,BGNC800 and BGNC900 (Fig.2) show only two typical diffraction peaks are observed in the range of 2θ of 5～90°,which are at 21° and 44° respectively correspond to the (002) and (101) diffraction peaks of graphite[30,31]. Compared with the standard graphite $2\theta \approx 26.6°$, the characteristic diffraction peak of sample clearly shifted leftward, according to the Prague formula: $2d \bullet \sin\theta = \lambda$[32], show that (002) the distance between the planes has been extended. Therefore, the BGNC700, BGNC800, and BGNC900 materials show an amorphous framework and low-degree graphitization. The low intensity and broadening (101) indicate that the BGNC800 consists of thin-carbon sheets. The high intensity in the low angle region is caused by the high mesopore density in the carbon sheets.

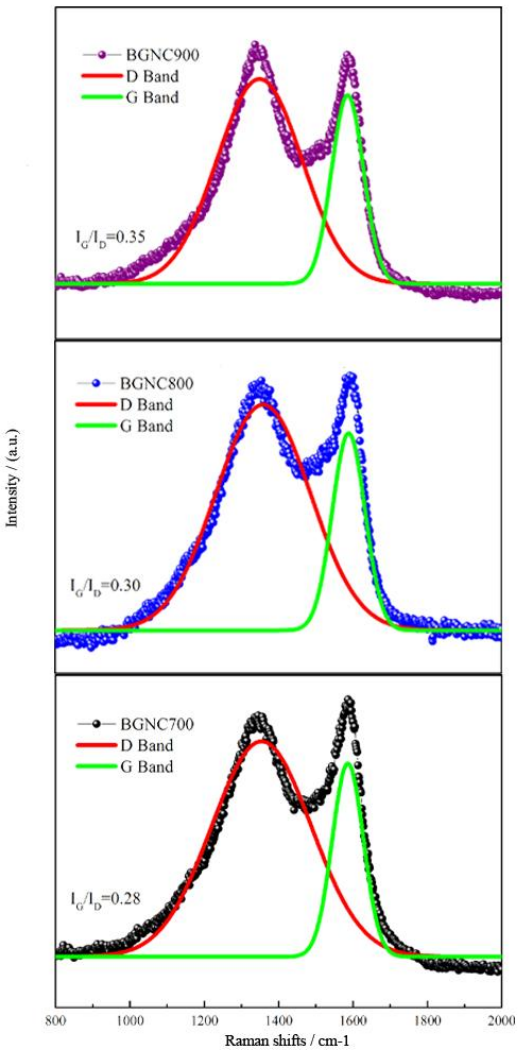

Figure 3. Raman spectra of BGNC.

Raman spectras was employed to confirm the graphitization degree of the investigated samples. As shown in the Fig.3, the spectra of BGNC display two obvious peaks, one is the G band located around 1589 cm^{-1} which was ascribed to the presence of a graphitic carbon phase and the E_{2g} phonon vibrations of sp^2 carbon atoms[33,34]. The other is disorder-induced D-band which located around 1348 cm^{-1} is associated with a double-resonance Raman process in disordered carbon,furthermore, the position and width of D-band may change depending on the structure, uniformity, and functional groups of the disordered carbon[35,36]. So, the area ratio between G and D bands (I_G/I_D) indicates the graphitization degree of the samples. As shown in Fig.3, obviously, With the increase of carbonization temperature, the value of I_G/I_D increases, and the degree of graphitization is gradually deepened. The full-width at half-maximumof both the G bands and D bands decreases with the increase of carbonization temperature, suggesting a structurally disordered carbon formed at a relatively low temperature.

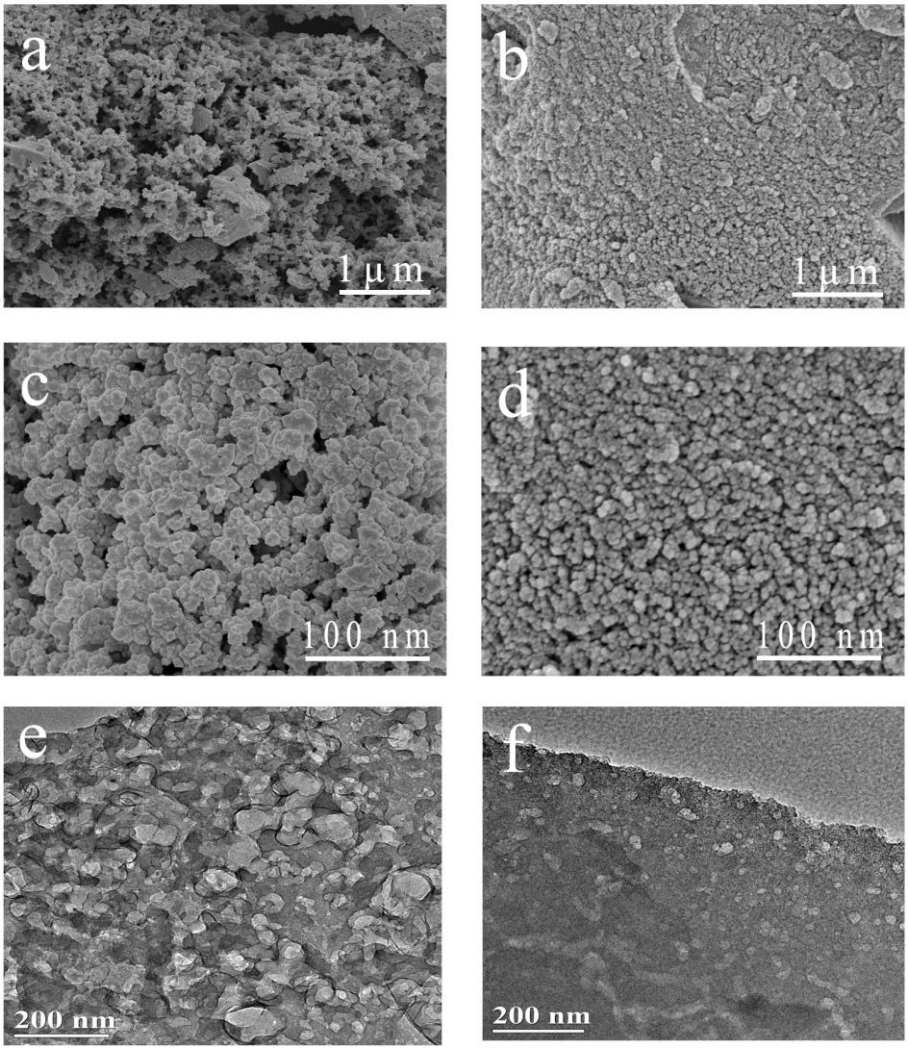

Figure 4. SEM images of BGNC800 (a,c) and NHBGNC(b,d); TEM images of BGNC800 (e) and NHBGNC(f)

The SEM images in Fig.1 shows that after the hydrothermal reaction, small carbon particles have been deposited to form a certain network frame structure. Fig.4a and 4c shows the low and high magnification SEM images of BGNC800, it is obvious that the in situ nitrogen-doped porous carbons were composed of intermixed nanoparticles, similar to the coral structure. The surface of the pores formed by the collapse of the pores can be observed in the accumulation of nano-particles for the microporous and mesoporous interwoven network structure. Fig.4b and 4d shows the low and high magnification SEM images of NHBGNC, the gap is relatively small, the hole structure is not rich as BGNC800 without hydrothermal treatment. The TEM image in Fig.4e and 4f further indicating that the BGNC800 has a dimensional mesh structure.

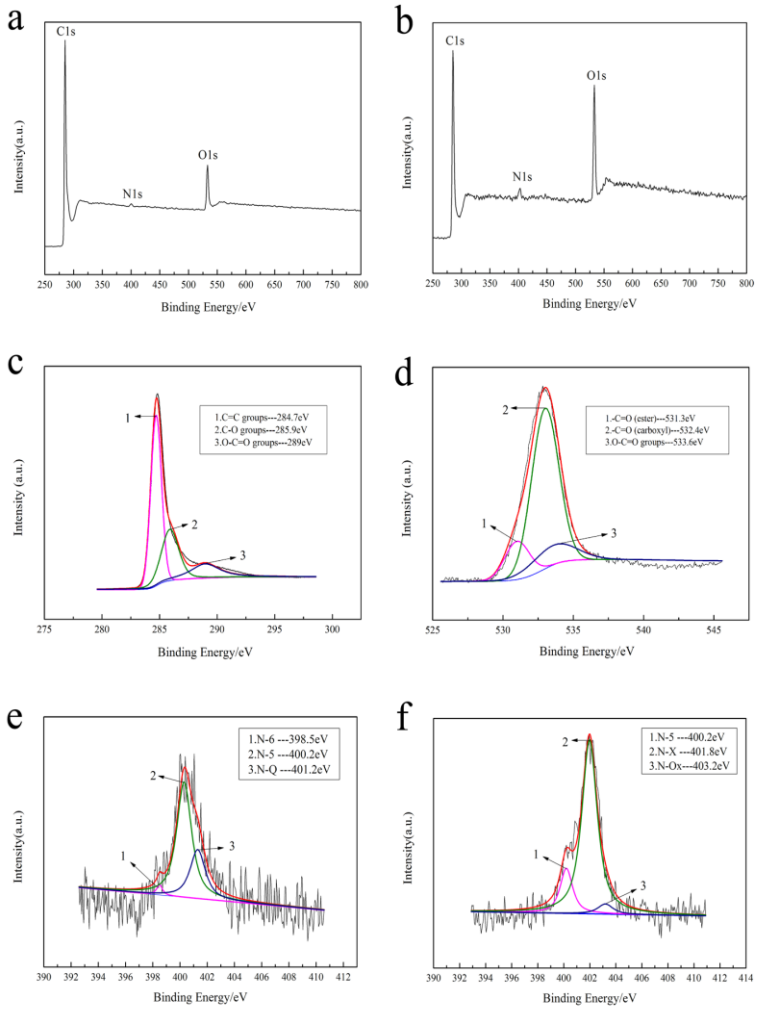

Figure 5. XPS survey and FTIR spectra of BGNC800 and NHBGNC(a,b), C*1s*(c), O*1s*(d), and N*1s* XPS spectra of BGNC800 and NHBGNC after fitting(e,f), FTIR spectra of BGNC800(g).

Table 1. Summary of XPS element content on BGNC800 and NHBGNC.

Contents	C	N	O	N-5
BGNC800	70.39 %	3.56 %	26.06 %	67.89 %
NHBGNC	57.38 %	4.56 %	38.06 %	16.47 %

X-ray photoelectron spectroscopy (XPS) was employed to determine the element compositions and chemical state of the prepared materials. A proposed structure of BGNC800 and NHBGNC on the basis of the XPS results is shown in Fig.5a and Fig.5b. The chemical features of C*1s*, N*1s*, and O*1s* suggest the successful formation of the in situ nitrogen-doped porous carbon materials after the carbonization of black garlic. The contents of the C,N and O dopants were quantified by their integrated peak areas, as shown in Table.1, calculation results of BGNC800 revealed the presence of

70.39 % carbon, 3.56 % nitrogen, and 26.05 % oxygen. The C*1s* spectrum can be fitted to three peaks ranging from 284.7 to 289 eV as shown in Fig.5c. Among that, the first peak about 284.7 eV is attributed to the C=C groups, the other two peaks located at 285.9 and 289.0 eV corresponded to C=O and O–C=O groups[37,38]. The O*1s* spectrum can be fitted to three peaks as shown in Fig.5d. The three peaks centered at 531.3, 532.4 and 533.6 eV were attributed to –C=O (ester), −C=O (carboxyl), O–C=O groups[39]. Furthermore, we found that abundant O element also are detected on BGNC800. The O content would result the corresponding improvement of O–contained functional groups on surface of carbon matrix, which would be helpful for the enhancement of surface wettability and thus improving the availability of micropores and small mesopores.

The N*1s* spectrum of BGNC800 and NHBGNC showed in Fig.5e and 5f can be fitted to five peaks at 398.5 eV, 400.2 eV, 401.2 eV, 401.8 eV, 403.2 eV, which can be designated to pyridine–N–6, pyrrole or pyridine–N–5, quaternary–N–Q, pyridine–N–oxide and chemisorbed nitrogen oxides–N–Ox, respectively. In KOH electrolyte, the main peak is attributed to N–5, which are identified as electrochemically active and electron donor tendency and thus enhance electrochemical capacitance of samples. The N–6 peak is bound to two carbon atoms and donates one p electron to the conjugation with the aromatic π–conjugated rings. As showed in Table.1, Although the nitrogen content of NHBGNC is higher than that of BGNC800, the N-5 content, which plays a critical role in the comparison of capacitance, is higher in BGNC800[20,40,41].

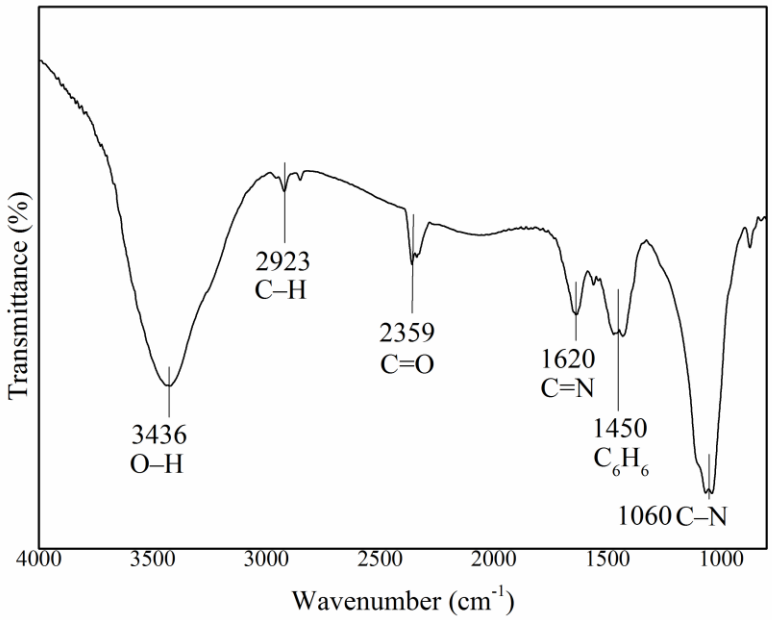

Figure 6. FTIR spectra of BGNC800.

The FTIR characterization exhibts the chemical groups of carbon materials derived from black garlic after carbonization. As showed in Fig.6, the BGNC is rich in oxygen-containing functional groups. The characteristic peaks at 3436 cm^{-1} are due to the stretching of hydroxyl peaks (O–H), which are present in all hydrothermal samples due to the fact that the main components of black garlic

contain hemicellulose, cellulose, And lignin, hydrothermal carbonation did not completely destroy the (O–H). The absorption peak at 2923 cm^{-1} is the aliphatic C–H bond (C–H in the cluster $–CH_3$, $–CH_2$). The intensities of the peaks at 2359 cm^{-1},1620 cm^{-1} and 1450 cm^{-1} which can be assigned to the stretching vibration of C=O groups, C=N groups stretching vibration and characteristic peaks of benzene ring structure[42-44]. The band at 1060 cm^{-1} has been observed in C–N vibrations, the covalent bond energy of C–N is much lower than that of C–C bonds. The release of abundant nitrogen atoms during the carbonization results in partial collapse of the carbon framework, leading to the decreasing pore size, specific surface area and pore volume[45].

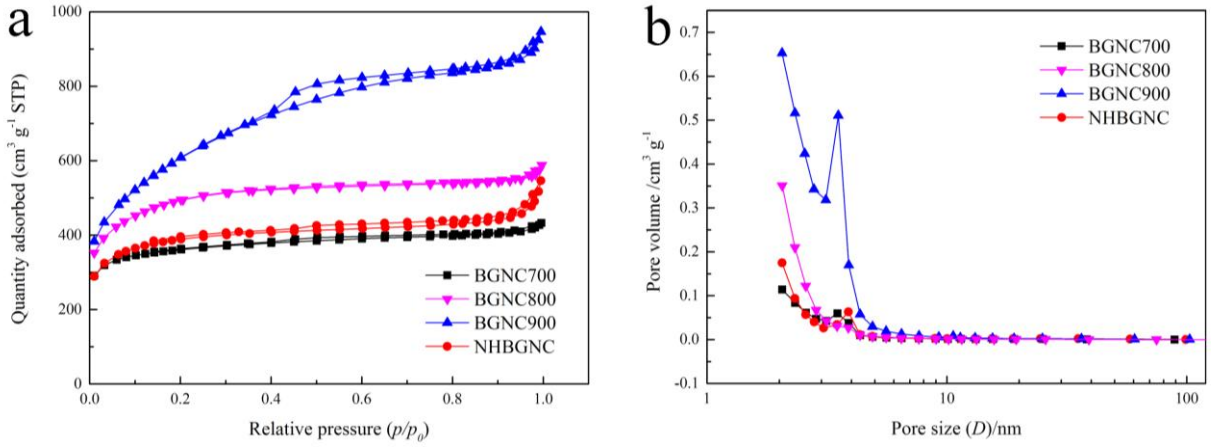

Figure 7. (a) N_2 adsorption/desorption isotherm and (b) the pore size distribution.

Table 2. Textural properties of the porous carbons obtained at different carbonization conditions.

Samples	Average Pore Sizes (nm)	S_{BET} (m^2 g^{-1})	Total PoreVolume (cm^3g^{-1})	Mesoporous Volume (cm^3g^{-1})	Microporous Volume (cm^3g^{-1})
BGNC700	2.10	1227	0.64	0.24	0.40
BGNC800	2.01	1714	0.86	0.46	0.40
BGNC900	2.52	2186	1.38	0.73	0.13
NHBGNC	2.20	1337	0.74	0.37	0.37

Nitrogen adsorption/desorption measurements was used to analyze the microstructure and pore structure of the porous carbon materials. The nitrogen adsorption/desorption curves of BGNC at different carbonization temperatures are shown in Fig.7a. The isotherm curves of the BGNCT present

the mixed type I and IV isotherm defined by the International Union of Pure and Applied Chemistry (IUPAC), indicating the presence of micro/mesopores[46]. The adsorbed N_2 volume significantly increased at a low pressure, this finding reveals the existence of a predominant amount of micropores within carbon. The type H4 hysteresis loop observed at a moderate pressure range in all curves revealed the presence of slit-shaped mesopores in the carbon. Fig.7b shows the pore size distribution obtained from the DFT method based on the adsorption branch of N_2 isotherms. The results shows the existence of both micropores and mesopores. The macropores and mesopores probably originated from the hydrothermal treatment, while the micropores and some small mesopores were generated by KOH chemical activation. At the same time, a significant increase in the pore volume of BGNC900 observed due to the presence of mesopores. As showed from Table.2, the average pore sizes of BGNCT (700,800,900) and NHBGNC is 2.10 , 2.01 ,2.52 and 2.20 nm. The potassium and hydroxide ions in the electrolyte are less than 0.4 nm[47]. Thus the size of these pores makes it easier for the electrolyte ions to go through and form the electric double layer capacitance. Meanwhile BGNC900 shows the largest specific surface area, but BGNC800 shows the best electrochemical performance. It because only the accessible surface area contributes to the specific capacitance. Thus, considering that the specific capacitance is contributed by the meso/macropores of the nitrogen-doped porous carbons at high scan rates and by micropores at low scan rates is reasonable[48]. Although the nitrogen content of NHBGNC is greater than that of BGNC800, the BGNC800 has better capacitive performance due to the specific surface area of BGNC800 and the large number of mes/microporous that result in more efficient ion transport.

3.2 Electrochemical performance of BGNC

Fig.8a shows the CV curves of BGNCT in 6 M KOH aqueous solutions at a scan rate of 10 mV s^{-1} in the potential window ranging from −1 to 0 V. All of the CV curves exhibited a nearly rectangular shape, indicating the good electrical properties. All samples exhibit a similar quasi-rectangular shape with a few redox peaks due to pseudocapacitive redox reactions of nitrogen-containing functional groups, which are attributed to both oxygen- and nitrogen-containing functional groups on the surface, these provide not only pseudo-capacitance via the redox reactions but also wettability by the electrolyte. As the hydrothermal treatment can retain a large number of nitrogen in the biomass and oxygen-containing functional groups, the BGNC800 displayed the largest integrated area surrounded by CV curves, indicating that this material also had the largest specific capacitance. Fig.8b shows the specific capacitances of the BGNC800 calculated from the CV curves at various scan rates, even at a high scan rate of 120 mV s^{-1} still maintain a higher specific capacitance of 246 F g^{-1}, indicating fast ion-transport into the electrochemically active surface and good capacitive behavior of electrode in quick charge–discharge operations[50,49].

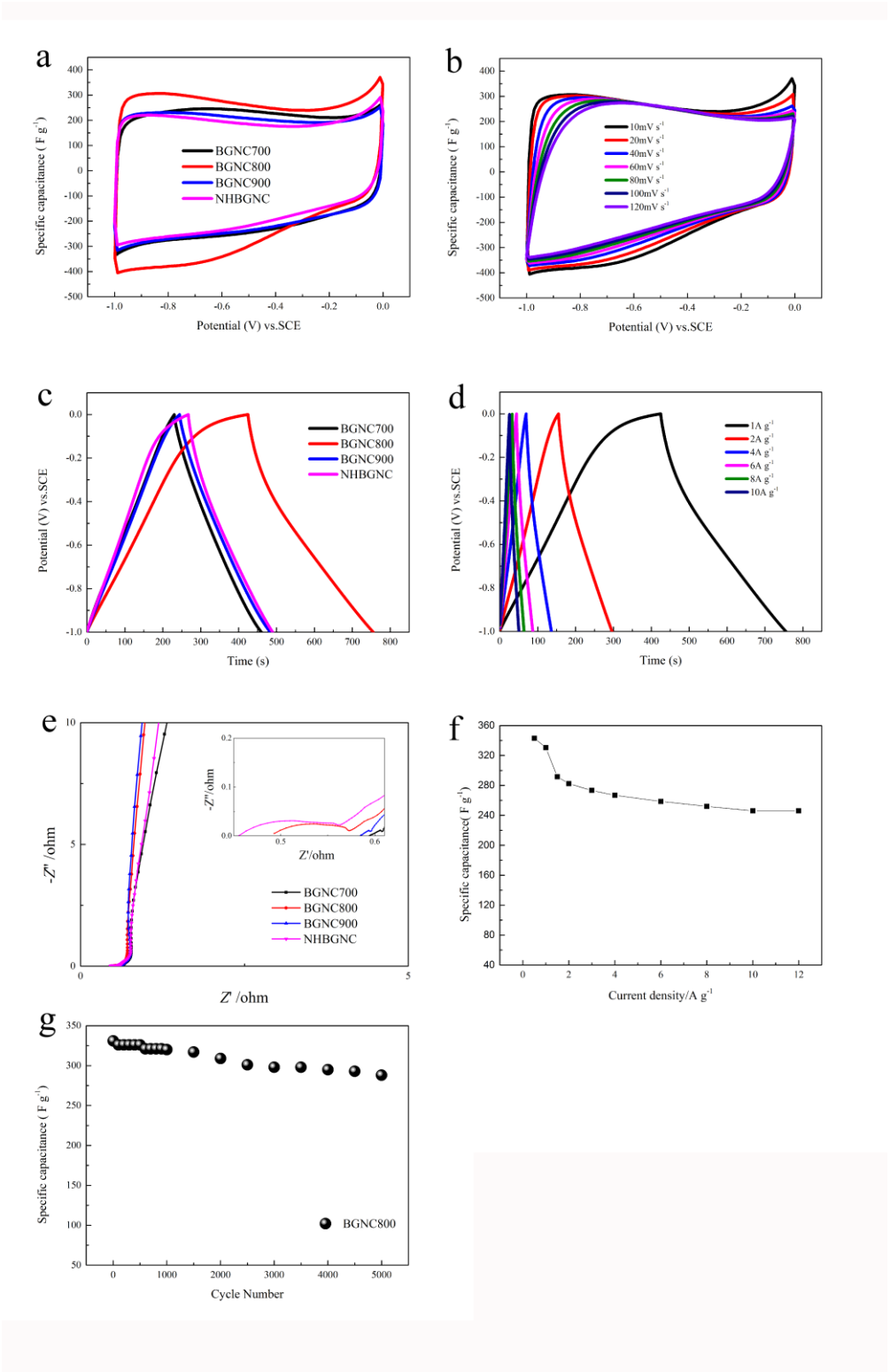

Figure 8. (a) The CV curves of BGNC700,800,900 and NHBGNC at the scanning rate of 10 mV s^{-1} (b) The CV curves at 8different scan rates from 10 to 80 mV s^{-1} of BGNC800 (c) The GCD curves of BGNC700,800,900 and NHBGNC at current density of 1 A g^{-1} (d) The GCD curves of the BGNC800 at different current densities from 1 to 10 A g^{-1} (e) Nyquist impedance plots of BGNC700,800,900 and NHBGNC (f) specific capacitance vs. current density of BGNC800 (g) The cycle performance of BGNC800 detected by PT at the scan rate of 1 A g^{-1}.

Table 3. Comparison of specific capacitance with various N-doped porous carbon electrode tested by three-electrode configuration.

Electrode materials	Electrolyte	Specific capacitance ($F g^{-1}$)	Ref.
fulvic acid potassium salts	6 mol KOH	235 F g^{-1}	[26]
cellulose aerogels	1 mol H_2SO_4	193 F g^{-1}	[32]
lignocellulosic	6 mol KOH	223.9 F g^{-1}	[37]
gelatin biomolecule	1 mol Na_2SO_4	254 F g^{-1}	[49]
black garlic	6 mol KOH	331 F g^{-1}	This work

Fig.8c shows the GCD curves of BGNCT measured at a current density of 1 A g^{-1}. All of these curves show nearly symmetric triangle shapes without any obvious voltage drop at the current density of 1 A g^{-1} and no obvious IR drops are observed in the charge–discharge curve of BGNCT, suggesting a tiny ohmic resistance and good coulombic efficiency. With abundant micropores and larger specific surface area (1714 $m^2 g^{-1}$), which offers plentiful adsorbing sits for ions, BGNC800 exhibits excellent capacitive behavior that a maximum specific capacitance of 331 F g^{-1} at a discharge current of 1 A g^{-1} (Fig.8d). It retained a capacitance of 246 F g^{-1} at a high current density of 10 A g^{-1} and capacitance retention is 85 % (Fig.8f) when the current density is increased 10 times, indicating the excellent electrochemical behavior and porosity of BGNC800.

Fig.8e demonstrates the Nyquist plots of BGNCT. The Nyquist plots show a nearly vertical in the low-frequency region and a well-defined semicircle in the high to medium frequency regions, indicating the relatively ideal capacitive performance of the materials. The AC-ESRs of BGNC in 6 mol KOH aqueous solution were 0.45 (NHBGNC), 0.49 (BGNC800), 0.58 (BGNC900) and 0.59 (BGNC700) Ω. The radius of the semicircle represents the pseudo-charge-transfer resistance. Clearly, BGNC800 in the 6 M KOH aqueous solution had a small pseudo-charge-transfer resistance. The cyclic stability of BGNC800 was measured at a constant discharge current density of 1 A g^{-1}. A high capacitance retention of 87.01 % was obtained even after charging/discharging for 5000 times, as shown in Fig. 8g. The high cycling durability of BGNC800 after 5000 cycles was believed to be related to its large BET surface area and optimal microstructure. The specific capacitance values of others similar nitrogen doped porous carbon electrodes recently reported in literatures also are presented in Table.3. As shown in Table.3, the specific capacitance value of the produced BGNC electrodes reaches 331 F g^{-1} under a current density of 1 A g^{-1}, respectively, indicating an efficiently enhanced charge storage capability for the produced BGNC electrodes. Meanwhile, more competitive charge storage capability than the similar porous carbon electrodes reported in literatures also is observed from Table.3.

4. CONCLUSION

In this study, black garlic derived in situ nitrogen doped porous carbon materials was obtained by hydrothermal - carbonization coupling method exhibits high specific capacitance of 331 F g^{-1} at a current density of 1 A g^{-1} in 6 M KOH solution, excellent rate performance with a capacitance retention of 85 % when the current density is increased 10 times and good stability with only capacitance decay of 12.99 % after 5000 cycles. The result offers a facile, low-cost and environmental-friendly approach to fabricate biomass derived in situ nitrogen doped high-capacitive porous carbon materials for commercial EDLC-related applications.

ACKNOWLEDGEMENT
This effort was supported by the National Natural Science Foundation of China (21364004 and 21664009), Gansu Province University Fundamental Research Funds and Doctor Research Fund of Lanzhou University of Technology, P.R. China.

References

1. J.R. Miller, P. Simon, *Science*, 321 (2008) 651
2. R. Liu, L. Wan, S. Liu, L. Pan, D. Wu, and D. Zhao, *Adv.Funct.Mater.*, 25 (2015) 526
3. J. Zhou, T. Zhu, W. Xing, Z. Li, H. Shen, and S. Zhuo, *Electrochim Acta.*, 160 (2015) 152
4. G. Lota, K. Fic, E. Frackowiak, *Energ. Environ. Sci.*, 4 (2011) 1592
5. P. Du, X. Hu, C. Yi, H.C. Liu, P. Liu, H.L. Zhang, and X. Gong, *Adv.Funct.Mater.*, 25 (2015) 2420
6. C. Zheng, X. Zhou, H. Cao, G. Wang, and Z. Liu, *J. Power. Sources.*, 258 (2014) 290
7. Z. Lin, X. Yan, J. Lang, R. Wang, and L.B. Kong, *J. Power. Sources.*, 279 (2015) 358
8. W. Qian, J. Zhu, Y. Zhang, X. Wu, and F. Yan, *Small*, 11 (2015) 4959
9. E. Frackowiak, F. Béguin, *Carbon*, 39 (2001) 937
10. W.H. Qu, Y.Y. Xu, A.H. Lu, X.Q. Zhang, and W.C. Li, *Bioresource Technol.*, 189 (2015) 285
11. D. Wang, S. Liu, G. Fang, G. Geng, and J. Ma, *Electrochim Acta.*, 216 (2016) 405
12. Y. Deng, Y. Xie, K. Zou, and X. Ji, *J. Mater. Chem A.*, 4 (2016) 1144
13. C. Han, X. Bo, Y. Zhang, M. Li, and L. Guo, *J. Power. Sources.*, 272 (2014) 267
14. A. Elmouwahidi, Z. Zapata-Benabithe, F. Carrasco-Marín, and C. Moreno-Castilla, *Bioresource Technol.*, 111 (2012) 185
15. D.S. Yuan, T.X. Zhou, S.L. Zhou, W.J. Zou, S.S. Mo, and N.N. Xia, *Electrochem Commun.*, 13 (2011) 242
16. C.L. Sun, H.W. Wang, M. Hayashi, L.C. Chen, and K.H. Chen, *J. Am. Chem. Soc.*, 128 (2006) 8368
17. K.A. Kurak, A.B. Anderson, *J. Phys. Chem. C.*, 113 (2009) 6730
18. J. Lahaye, G. Nansé, A. Bagreev, and V. Strelko, *Carbon*, 37 (1999) 585
19. J.P. Paraknowitsch, A. Thomas, and M. Antonietti, *J. Mater. Chem.*, 20 (2010) 6746
20. R.J.J. Jansen, H.V. Bekkum, *Carbon*, 33 (1995) 1021
21. G. Ma, Q. Yang, K. Sun, H. Peng, F. Ran, X. Zhao, and Z. Lei, *Bioresource Technol.*, 197 (2015) 137
22. B. Zou, Y. Zhang, L. Xiao, and T. Li, *Energ. Environ. Sci.*, 3 (2010) 1437
23. Y. Shao, X. Wang, M. Engelhard, C. Wang, S. Dai, J. Liu, Z. Yang, and Y. Lin, *J. Power. Sources.*, 195 (2010) 4375
24. C. Liang, S. Dai, *J. Am. Chem. Soc.*, 128 (2006) 5316
25. E.G. Gillan, *Chem Mater.*, 12 (2000) 3906

26. Y.Z. Chen, P. Li, X. Zhao, J.Q. Zhang, and H.M. Luo, *J. Solid. State. Electrochem.*, 21 (2016) 171
27. J.E. Hodge, *J. Agr. Food. Chem.*, 1 (1953) 625
28. H.M. Lee, G.H. Jeong, D.W. Kang, S.W. Kim, and C.K. Kim, *J. Power. Sources.*, 281 (2015) 44
29. J. Yan, Q. Wang, T. Wei, Z. Fan, *Adv. Energy. Mater.*, 4 (2014) 157
30. X. Chen, B. Zhao, Y. Cai, M.O. Tadé, and Z. Shao, *Nanoscale*, 5 (2013) 12589
31. Z. Chen, X. Peng, X. Zhang, S. Jing, L. Zhong, and R. Sun, *Carbohydr Polym.*, (2017) 107
32. W. Yong, F. Su, C.D. Wood, J.Y. Lee and X.S. Zhao, *Ind. Eng. Chem. Res.*, 47 (2008) 2294
33. A. Sadezky, H. Muckenhuber, H. Grothe, R. Niessner, and U. Pöschl, *Carbon*, 43 (2005) 1731
34. A.C. Ferrari, J. Robertson, *Phys. Rev. B. Condens. Matter.*, 61 (2000) 14095
35. A. Kajdos, A. Kvit, F. Jones, J. Jagiello, and G. Yushin, *J. Am. Chem. Soc.*, 132 (2010) 3252
36. S. Zhang, K. Tian, B.H. Cheng, and H. Jiang, *ACS. Sustain. Chem. Eng.*, 5 (2017) 6682
37. V. Datsyuk, M. Kalyva, K. Papagelis, J. Parthenios, D. Tasis, A. Siokou, I. Kallitsis, and C. Galiotis, *Carbon*, 46 (2008) 833
38. F. Ye, B. Zhao, R. Ran, and Z. Shao, *Chemistry (Weinheim an der Bergstrasse, Germany)*, 20 (2014) 4055
39. D. Hulicova-Jurcakova, M. Seredych, Q.L. Gao, and T.J. Bandosz, *Adv. Funct. Mater.*, 19 (2009) 438
40. X. Fan, L. Zhang, G. Zhang, Z. Shu, and J. Shi, *Carbon*, 61 (2013) 423
41. A. Sánchez-Sánchez, F. Suárez-García, A. Martínez-Alonso, and J. Tascón, *Carbon*, 70 (2014) 119
42. V. Khomenko, E. Raymundo-Piñero, and F. Béguin, *J. Power. Sources.*, 195 (2010) 4234
43. X. Yuan, S. Xu, J. Lü, X. Yan, L. Hu, and Q. Xue, *Micropor. Mesopor. Mater.*, 138 (2011) 40
44. P.A. Bazuła, A.H. Lu, J.J. Nitz, and F. Schüth, *Micropor. Mesopor. Mater.*, 108 (2008) 266
45. J. Zhang, L.B. Kong, J.J. Cai, H. Li, Y.C. Luo, L. Kang, *Micropor. Mesopor. Mater.*, 132 (2010) 154
46. F. Li, M. Morris, K.Y. Chan, *J. Mater. Chem.*, 21 (2011) 8880
47. G. Zhou, D.W. Wang, F. Li, L. Zhang, N. Li, Z.S. Wu, L. Wen, G.Q. Lu, and H.M. Cheng, *Chem Mater.*, 22 (2010) 5306
48. L.L. Zhang, X.S. Zhao, *Chem. Soc. Rev.*, 38 (2009) 2520
49. H.L. Jiang, B. Liu, Y.Q. Lan, K. Kuratani, T. Akita, H. Shioyama, F. Zong, and Q. Xu, *J. Am. Chem. Soc.*, 133 (2011) 11854
50. D.S. Dhawale, G.P. Mane, S. Joseph, C. Anand, K. Ariga, and A. Vinu, *Chemphyschem*, 14 (2013) 1563